



A relationship between rain radar reflectivity and height elevation variance of ringwaves due to the impact of rain on the sea surface

P. Sobieski,¹ C. Craeye,¹ and L. F. Bliven²

Received 18 April 2008; revised 2 December 2008; accepted 25 February 2009; published 15 May 2009.

[1] Raindrops impacting the rough sea modify its surface and its backscattering coefficient. This roughness change essentially depends on the rain content in very large drops, which is highly variable from one drop size distribution model to another. However, it has been observed that the radar reflectivity of raindrops has a drop size dependence very similar to that of the ringwaves induced by rain on the surface. From a numerical analysis on various drop size distributions, rain rates, and frequencies from 3 to 35 GHz, a relationship between the sea surface elevation variance of ringwaves resulting from drop impact and the rain radar reflectivity Z is established. It is found to be weakly dependent on the raindrop size distribution model. This link is expected to lead to better estimates of the surface roughness, and in turn, via electromagnetic scattering models, it could improve algorithms for near nadir rain radar retrieval.

Citation: Sobieski, P., C. Craeye, and L. F. Bliven (2009), A relationship between rain radar reflectivity and height elevation variance of ringwaves due to the impact of rain on the sea surface, *Radio Sci.*, 44, RS3005, doi:10.1029/2008RS003880.

1. Introduction

[2] The measurement of rain has always been of great interest for human activities and its significance has increased in view of climatic challenges. Global rain monitoring became possible with microwave ground based remote sensing techniques like weather radars, as well as with the launch of remote sensing satellites. Major achievements have been reached thanks to several satellite missions with payloads containing multifrequency radiometers, and more recently the successful TRMM mission. Future perspectives are ahead with the Global Precipitation Mission (GPM) (R. K. Kakar et al., Global Precipitation Measurement (GPM) progress, paper presented at 2nd International GPM Ground Validation Workshop, National Taiwan University, Taipei, Taiwan, 2005) planned for the near future. The core instrument on TRMM as in GPM is a precipitation radar (PR) that measures the rain reflectivity Z from space at or near nadir.

[3] To determine accurate rain profiles a resolution high enough, consistent with rain cell sizes, is needed. For ground based stations the antenna size and transmitted power are not limiting factors as it is the case for spaceborne payloads. Therefore in ground based radars non attenuating low microwave frequencies can be used while space radars will have to use higher but attenuating frequencies.

[4] The algorithms retrieving vertical rain profiles from apparent Z obtained by rain radars often make use of power law relationships between rain rate R , specific attenuation k and reflectivity Z . These are basically marching-on procedures in which Z_i at each gate i is used to estimate the corresponding rain rate R_i , and in turn, the attenuation k_i necessary to correct the apparent Z_{i+1} in the next gate $i + 1$ for the two-way path attenuation. It is known that such procedures, like the classical H-B algorithm [Hirschfeld and Bordan, 1954], suffer from significant propagation errors and instabilities due to the fact that, among others, the first gates correspond to the 0°C isotherm where mixed rain and melting hydrometeors coexist. This affects the classical rain only relationships and introduces significant uncertainties. Therefore researchers introduced additional constraints in order to stabilize the retrieval algorithms. A possible constraint is the total PIA (Path Integrated Attenuation) that can be exploited in different forward

¹Telecommunications and Remote Sensing Laboratory, Université catholique de Louvain, Louvain-la-Neuve, Belgium.

²Wallops Flight Facility, NASA Goddard Space Flight Center, Wallops Island, Virginia, USA.

or backward techniques like the SRT (Surface Reference Technique) and companion methods for a single frequency PR [Iguchi *et al.*, 2000; Meneghini *et al.*, 2001], the DSRT (Dual Surface Reference Technique) or the DWT (Dual Wavelength Technique) for a dual frequency PR [Kozu *et al.*, 1991; Meneghini *et al.*, 1992; Nakamura and Iguchi, 2007].

[5] The two-way PIA may be evaluated from various sources, like collocated radiometric measurements or, when the PR flies above the ocean, from the estimate of the attenuation of the ocean surface echo inside rain, provided that a good estimate of the surface reflectivity may be found. One way to obtain this information is to use the surface reflectivity of the ocean just outside the rain cell as a reference [Meneghini *et al.*, 2001; Ferreira *et al.*, 2001; Durden *et al.*, 2003; Meneghini and Liao, 2007]. In this technique, the backscattering coefficients of the surface σ° inside rain and outside rain are assumed to be equal. However, it is well known that the impact of raindrops on the sea surface significantly modifies its backscattering coefficient [Moore *et al.*, 1979]. The purpose of this paper is to contribute to further improvements of rain radar retrieval algorithms by establishing an additional link between the ocean surface echo perturbed by rain and the rain reflectivity above the surface. The idea is based on the observation that those two quantities have similar dependence on drop size distribution (DSD).

[6] This paper is organized as follows: the perturbation of the sea surface by the rain impact is analyzed (section 2) in order to derive the dependence of the rain-induced surface variance on the drop size distribution (section 3). A selection of DSDs is presented (section 4) and the similarities between the rain-induced surface variance and the rain reflectivity dependencies versus the DSD are highlighted. Numerical simulations of both quantities versus rain rate for various DSDs (section 5) lead after a selection procedure to a polynomial identification linking directly surface variance and rain reflectivity (section 6).

2. Sea Surface Perturbation by Rain

[7] The impact of rain on a water surface significantly modifies its roughness and, in turn, its reflectivity. It is well known that rain simultaneously damps the sea surface waves and produces additional roughness. These effects introduce biases on wind speed estimates from scatterometers [Guymer *et al.*, 1981; Black *et al.*, 1985; Stiles and Yueh, 2002] and modify SAR images [Atlas, 1994; Melsheimer *et al.*, 2001; Alpers and Lin, 2006].

[8] As for the surface roughening, when a single raindrop hits a quiet water surface, it generates a crater with a crown which collapses to form a vertical stalk of water, and then subsides to spawn rings of gravity-

capillary waves [Worthington, 1963; Le Méhauté *et al.*, 1987; Le Méhauté, 1988]. Hallett and Christensen [1984] and Rein [1993] analyzed these features through high-speed photography, while Hansen [1986] combined such observations with high-resolution radar measurements at 9 GHz and grazing angles for individual splashes. Stalks have been identified as the dominant feature for backscattered power at grazing angles for individual drops of 3 and 4 mm [Wetzel, 1990].

[9] Besides the splash products, rain also damps the sea waves if the rain intensity is high enough. The very first study of this effect seems to be that of Reynolds [1900], who in 1875 mentioned the damping effect of sea waves by rain which is well known to sailors. This damping has been modeled by Manton [1973], who established an “eddy viscosity” of water related to the turbulence induced by the raindrop impacts. Wavetank experiments under very heavy artificial rain (150–600 mm/h at 50% of drop terminal velocity) by Tsimplis and Thorpe [1989] allowed them to estimate the eddy viscosity [Tsimplis, 1992]. Nyvsten [1990] extended the modeling of the damping effect to a two-layer surface wave model of a turbulent layer overlaying a second nonturbulent one.

[10] Wavetank experiments with high-speed photography of surface features induced by single drop impacts falling very close to terminal velocity (within 1%) have further been performed, together with scattering measurements. These wavetank measurements have been extended to the surface backscattering in case of monodisperse and polydisperse artificial rains, with drops falling also at terminal velocity. Experiments to analyze the drop size dependence have been conducted as well [Bliven *et al.*, 1993; Sobieski and Bliven, 1995; Bliven *et al.*, 1997; Sobieski *et al.*, 1999]. These have shown that, at scatterometric incidences (30° from nadir), the dominant features of backscattered power due to the impact of drops are not the stalks but the generated ringwaves. These yield an additional component in the surface elevation spectrum, superimposed to the surface spectrum due to instantaneous wind speed and wind history.

[11] Multifrequency (S, C and X bands) and multi-polarization scatterometric and Doppler measurements, in laboratory as well as in open field, along with rain data confirmed the previous findings. More specifically extensive measurements by Braun *et al.* [2002] and Braun and Gade [2006] indicated that the dominant scattering mechanism of a rain-roughened water surface observed at all incidence angles at VV polarization is Bragg scattering from ringwaves. For HH polarization, the radar backscattering mechanisms are dependent on incidence angle: at steep incidences Bragg scattering from ringwaves is dominant, while with increasing angle this effect diminishes and scattering from nonpropagating

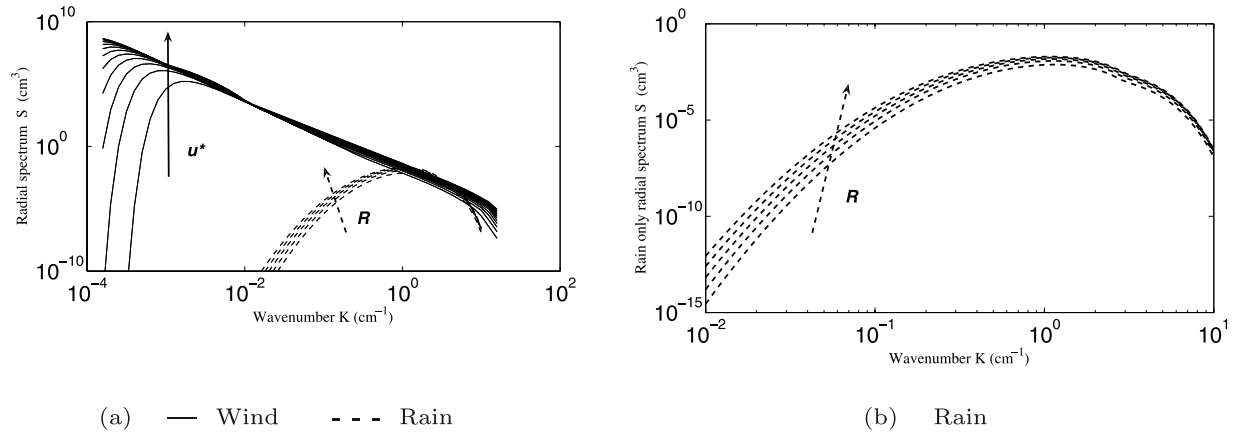


Figure 1. (a) Wind only and rain only radial sea surface elevation spectra $S(K)$ for increasing wind friction velocities u_* and rain rates R . u_* ranges from 20 to 120 cm/s by steps of 10 cm/s and R ranges from 20 to 100 mm/h by steps of 20 mm/h. (b) Rain only component.

splash products, like stalks, becomes more visible, as delineated from the conclusions of *Wetzel* [1990].

[12] Ku band measurements during the KWAJEX experiment, as well as on the Cowlitz river by *Contreras et al.* [2003] and *Contreras and Plant* [2004], extended the previous results to open field rain conditions. They concluded from Doppler spectra that VV backscatter during rain is mainly due to ringwaves, while HH backscatter is also from ringwaves at moderate incidence angles (20° – 60°) but contains substantial contributions from stationary splash products at high incidence angles.

[13] One significant outcome of these studies lies in the fact that for incidence angles not too far from nadir the rain effect appears, first, to be mostly related to the roughening of the surface due to ringwaves, and second, that this effect may reasonably be considered as additive. This approximatively additive characteristic allowed *Draper and Long* [2004a, 2004b] to retrieve both wind and rain fields from SeaWinds data. On the contrary for higher incidence angles it is probably the combined effect of both ringwaves and stalks may cause significant increases in sea surface radar cross section as can be suggested from the data collected by *Weissman and Bourassa* [2008].

[14] In this paper, we focus on the change of the sea surface spectrum of the surface displacements in presence of rain and wind. A model for the additive spectral component to the wind spectrum due to the presence of the ringwaves has been derived for monodisperse rain by *Bliven et al.* [1997] and *Craeye et al.* [1997]. The wind only radial spectrum $S(K)$, where K is the wave number (cm^{-1}) and this additional component due to rain are shown in Figure 1 for increasing wind friction velocities u_* and rain rates R . The wind spectrum shown here is

obtained from *Lemaire et al.* [1999], but could be replaced by other models available in the literature [e.g., *Elfouhaily et al.*, 1997]. Figure 1b shows the details of the rain radial spectrum in the frequency domain for the monodisperse case (2.8 mm diameter drops) whose analytical expression is given by *Lemaire et al.* [2002] for various drop sizes.

[15] The elevation variance can be written as:

$$\sigma^2 = \int_0^\infty S_K(K) dK = \int_0^\infty S_f(f) df \quad (1)$$

[16] It should be noted that nonlinear combinations of rain and wind spectra have also been studied by *Craeye* [1998] and recently in the very comprehensive paper by *Contreras and Plant* [2006]. However, this aspect will be left outside the scope of this paper, which looks for a direct relationship between the elevation variance σ^2 of the ringwaves and the drop reflectivity Z .

3. Dependence of Rain-Induced Surface Variance on DSD

[17] Experiments with single drops by *Craeye et al.* [1999] have shown that the energy transferred by the drop into surface ringwaves is not proportional to the kinetic energy of the drop. Indeed, it was observed that the largest drops have a much larger relative contribution to the surface elevation variance than small ones. In other words, for large drops, a much larger fraction of the incident kinetic energy is transformed into surface waves. More precisely, this study has shown that the contribution of a given drop to the surface elevation

variance is nearly proportional to the square of its momentum m^2v^2 . Other experimental data obtained for various monodisperse artificial rain events, with various drops sizes [Lemaire *et al.*, 2002], confirmed the drop size scaling rule based on the squared momentum law. In the following paragraphs, we provide three steps supporting the squared momentum model.

3.1. Step 1: Single Drop

[18] Let us first define the normalized surface energy $E(t)$ (dimensions m^2) of a ringwave generated by a drop after an impact at time $t = 0$:

$$E(t) = \int_{surf} z^2(\vec{r}, t) dS = 2\pi \int z^2(r, t) r dr$$

$$\simeq E_o e^{-t/\tau} \quad t > 0 \quad (2)$$

where r is the horizontal distance from the point of impact, $z(r, t)$ is the water height and the integral over dS is taken over the horizontal surface where the ringwave extends. Owing to the viscosity of water, we may expect an exponential decay of energy versus time. The corresponding lifetime is denoted by τ . This exponential decay is a mere approximation, among others, because the ringwaves need to be fully developed (the point of impact is almost at rest again) for this model to be reasonable. Nevertheless, the reasoning below holds with a more accurate time dependence than the exponential model above.

[19] Let us denote by $K = mv^2/2$ the kinetic energy of the impacting drop. As will be detailed below, the fraction of the drop kinetic energy transferred to surface waves, i.e., the E_o/K ratio, is not constant and exhibits a strong dependence on drop size. Actually, it appears that, in good approximation, this fraction increases linearly with the volume (or mass) of the drop. This point can be deduced from *Le Méhauté* [1988], where the amplitude z of the wave is found to be proportional to $m v$. This indeed leads to a value of E_o proportional to m^2v^2 , and in turn, a E_o/K ratio proportional to m . Measurements presented by *Craeye et al.* [1999] for two different drop sizes support this relationship. This is also quantitatively consistent for the full monodisperse rain case [Lemaire *et al.*, 2002], analyzed hereafter. In the following, we will use the model:

$$E_o = Cm^2v^2 = C_1D^6v^2 \quad (3)$$

where D is the drop size (mm) and the proportionality constants C and C_1 are with dimensions $kg^{-2}s^2$ and $m^{-6}s^2$, respectively.

3.2. Step 2: Full Monodisperse Rain

[20] We now consider rain with constant drop size D . If N_{mono} is the density of falling drops in air (in m^{-3}), and $v(D)$

is their velocity, the number n_o of drops that hit a unitary surface per unit of time (in $m^{-2}s^{-1}$) can be obtained as:

$$n_o = N_{mono} v(D) \quad (4)$$

[21] Alternatively, if the rain rate R (in $mm h^{-1}$) is known, we also have:

$$n_o = \frac{\chi R}{D^3} \quad (5)$$

where χ is a constant equal to 530, expressed in $mm^2 m^{-2} h s^{-1}$. The normalized surface energy generated by an individual drop may be written as:

$$E_i(t) = \int_{surf} z(t)^2 dS = E_o f_o(t - \tau_i) \quad (6)$$

where, in first approximation, $f_o(t) = e^{-t/\tau}$ for $t > 0$ and $f_o = 0$ for $t < 0$. Therefore, if we consider the surface as the superposition of individual ringwaves, the average total normalized energy can be obtained by assuming ergodicity of the height random variable. Doing so, we obtain the elevation variance as:

$$\sigma^2 = \lim_{T \rightarrow \infty} \frac{1}{T} \int_0^T \sum_i^{n_o} E_i(t) dt \quad (7)$$

[22] Using the expressions above for the number n_o of drops impacting a unit surface per unit of time, we obtain two possible expressions for the elevation variance:

$$\sigma^2 = E_o n_o \tau = Cm^2v^2 N_{mono} v \tau = C_1 D^6 v^3 N_{mono} \tau \quad (8)$$

and

$$\sigma^2 = Cm^2v^2 \frac{530R}{D^3} \tau = C_1 D^3 v^2 530R \tau \quad (9)$$

[23] This shows that once σ^2 is known along with the characteristics of falling drops (R, D, v) the product $C_1\tau$ can be found.

[24] Expression (8) will be extended in the next section to natural rain conditions. The drop size dependence of expression (9) has been found consistent with data presented by *Lemaire et al.* [2002], where elevation variances obtained with identical rain rates and different drop sizes are compared. This further supports model (3).

[25] It should be noted that the expressions above still hold for a nonexponential decay of the energy brought to the surface by a single drop. In this case, the lifetime must be defined as:

$$\tau = \int_0^\infty f_o(t) dt \quad (10)$$

where f_o is defined above and has a maximum value equal to 1.

3.3. Step 3: Natural Rain

[26] Natural rain is characterized by its drop size distribution (DSD) $N(D)$, defined in such a way that $N(D) dD$ is the number of drops per m^3 with a size in the interval $[D - dD/2, D + dD/2]$. Following the reasoning of the previous paragraph, it can be assumed that each drop brings to the surface an energy proportional to its squared momentum $E_o = C_1 D^6 v^2(D)$, and that this energy lasts for a given time τ . The number of drops, with a size in the interval $[D - dD/2, D + dD/2]$, that hit a unit surface per unit of time is $v(D) N(D) dD$. The integration of individual ringwave energies over the distribution of drops that hit the surface then yields:

$$\sigma^2 = \int_0^\infty C_1 D^6 v^2(D) \tau v(D) N(D) dD \quad (11)$$

which shows a $D^6 v^3(D)$ dependence for the ringwaves height variance.

[27] From the studies by *Craeye* [1998] and *Lemaire et al.* [2002], we found that $\tau(R)$ may be obtained from monodisperse rain experimental data. These allowed us to estimate the product $C_1 \tau$ and to approximate this quantity by the following exponential function:

$$C_1 \tau(R) = 1.18 \cdot 10^{-7} e^{(-10.34 \cdot 10^{-3} R + 25.23 \cdot 10^{-6} R^2)} \quad (12)$$

for $R < 150 \text{ mm/h}$

which is a slowly decreasing function of rain rate up to values of $R \simeq 100 \text{ mm/h}$. For light rain rates, $\tau(R)$ appears almost constant, because interactions are negligible, while it tends to become smaller when the rain rate increases, because of an increase of turbulence and dissipation rate. From this weak dependence for monodisperse rains, we also concluded that the lifetime may be assumed to depend on the rain rate R only, which implies that the surface elevation variance σ^2 may be written as:

$$\sigma^2 = C_1 \tau(R) \int_0^\infty D^6 v^3(D) N(D, R) dD \quad (13)$$

and thus depends on the sixth power of D and the third power of terminal velocity $v(D)$. This drop velocity in rain is a well known quantity [*Gunn and Kinzer*, 1949]. Owing to air friction effects, it presents a rather low dependence on drop diameter D and a saturation effect for large drops with a terminal drop velocity $v(D) \simeq 9 \text{ m/s}$.

[28] For the sake of completeness and to highlight the consistency of this model, it should still be noted that the results from *Le Méhauté* [1988] and *Sobieski et al.*

[1999] have been exploited to reproduce scattering data by *Contreras and Plant* [2006], based on tuning of the ringwave maximum age and of the radius of the drop impulse. With this procedure, they obtained ringwave lifetimes of about $\tau = 4 \text{ s}$ to match observations from the KWAJEX campaign.

4. Dependence of Rain Radar Reflectivity on DSD

[29] For scattering by particles that are very small compared to the wavelength λ , the Rayleigh approximation holds, and the backscattering cross section is proportional to the sixth power of the drop diameter D . However the conditions for the Rayleigh scattering approximation are not necessarily fulfilled in existing and future satellite configurations. Hence, exact Mie computations are necessary, and the rain radar reflectivity will take a modified form:

$$Z = \int_0^\infty f(D) N(D, R) dD \quad (14)$$

with $f(D) \approx cD^6$ only if $D \ll \lambda$

[30] The functional similarity between the surface elevation variance and the atmospheric drop reflectivity in equations (13) and (14) is striking. Obviously, both quantities resemble the sixth moment of the DSD, which makes them highly sensitive on the very large drop content, for which the terminal velocity $v(D)$ is almost constant. However, it is well known that different rain events may have the same rain rate, but quite different DSDs. Hence, there will be no unique relationship between rain rate and surface energy, as is also the case between rain rate and reflectivity. Therefore let us derive a direct relationship between the calculated surface energy σ^2 and the rain reflectivity Z , in order to analyze its dependence on the choice of the drop size distribution, and especially for their large drops content.

[31] The evolution of raindrop sizes is governed by complex processes, depending on many parameters changing from the source region in clouds to the bottom of the atmosphere. Attempts to quantify DSDs are mostly empirical and many contributions have been made by numerous authors for the various climate regions and cloud types around the globe (specified by ITU-R). It is not the purpose here to review all the experience gained in that field over decades. Our approach has been to exploit the results of a systematic compilation and analysis of numerous models made by *Montanari* [1997] relevant for our study. As research is going on, new parameterizations of the DSD regularly appear and will continue to do so. Here, we limit ourself to assess

the relationships between σ^2 , Z and R on a sufficiently wide range of reasonably well accepted DSD models.

[32] Several functional forms can be used to fit an experimental DSD. Having in mind our further classification and selection purposes, let us organize them according to exponential, Gamma, lognormal or Weibull types. Because exponential functions are simple, their use has been attractive and has led to a long tradition in rain radar applications:

$$N(D, R) = N_0 \exp(-\Lambda(R)D) \quad (15)$$

with $\Lambda(R) = 4.1 R^{-0.21}$

[33] The above exponential distribution introduced by *Marshall and Palmer* [1948] has only two parameters N_0 and $\Lambda(R)$. Some observations, however, indicated that natural rain DSDs contain fewer of both very large and very small drops than predicted by the exponential distribution. For this purpose, a generalized Gamma distribution for representing raindrop spectra has been proposed:

$$N(D, R) = N_0 D^\mu \exp(-\Lambda D) \quad (16)$$

The Gamma DSD has three parameters N_0 , μ , $\Lambda(R)$ and allows to describe a broader range of DSDs than the exponential law, which then becomes a special case of a Gamma distribution with $\mu = 0$. An extensive analysis of this distribution and of its impact on the coefficients in the power law relationship between rain specific attenuation k and the rain rate R may be found in the work of *Haddad et al.* [2004], where new parameterizations are proposed.

[34] This Gamma DSD has been further extended to provide more degrees of freedom to fit measurements:

$$N(D, R) = \frac{N_T}{\Gamma(c) b^c} D^{c-1} \exp\left(-\frac{D}{b}\right) \quad (17)$$

The parameter N_T accounts for the density number of drops, while b and c stand for the mean diameter and the skewness of drops, respectively. These quantities may be expressed as power laws of the rain rate R .

[35] Although not as widely used as the various forms of the Gamma distribution, the lognormal DSD given hereafter has found applications to both rain and cloud measurements. This distribution may be written as:

$$N(D, R) = \frac{N_t}{D \sqrt{2\pi\sigma_n^2}} \exp\left[-\frac{(\ln D - \mu)^2}{2\sigma_n^2}\right] \quad (18)$$

$$\mu = \mu_a + \mu_b \ln(R) \quad (19)$$

$$\sigma_n^2 = |\sigma_a^2 + \sigma_b^2 \ln(R)| \quad (20)$$

In equation (19), μ_a and μ_b represent a logarithmic average of diameters, while σ_a and σ_b in (20) are their standard deviations. In convective rain events, μ is always positive, varying from 0 to 0.5, whereas in stratiform cases, μ takes both positive and negative values between -1.5 and 1.5 . No marked boundaries in N_T and σ_n^2 are noticed in either type of rainfall. However, above 100 mm/h, σ_n^2 is almost independent from rain rate [*Timothy et al.*, 2002].

[36] Under heavy rainfall rates, the Gamma and the lognormal laws give somewhat similar results; however, as mentioned by *Montanari* [1997], the lognormal model fits the measurements better than any other distribution.

[37] The Weibull DSD is practical for rainfall composed mostly of small particles. This function is also claimed to provide good comparative results with measured attenuation and rainfall rate. It is given by:

$$N(D, R) = N_T \frac{c}{b} \left(\frac{D}{b}\right)^{c-1} \exp\left[-\left(\frac{D}{b}\right)^c\right] \quad (21)$$

[38] Table 1 summarizes a large set of models gathered for the various world climatic regions. Many of them are quoted from *Montanari's* [1997] compilation. A few others correspond to *Li et al.* [1994], *Timothy et al.* [2002], and *Maciel and Assis* [1990] not included in the *Montanari* compilation.

[39] It should be stressed that Table 1 is obviously not exhaustive, as further interesting work on DSD is going on [*Uijlenhoet*, 2001; *Zhang et al.*, 2001; *Hendrantoro and Zawadzki*, 2003]. Figure 2 displays 26 DSDs in two groups: the exponential and the Gamma DSDs (Figure 2, left), and the lognormal and the Weibull ones (Figure 2, right). In the next section these DSD will not all be exploited, but a selection will be made in the context of the searched goal: the design of a σ^2 vs Z relationship.

5. Selection Criteria on DSDs

[40] Figure 2 highlights the fact that some DSDs (dotted lines) present a very particular behavior that could introduce a large bias when deriving a general relationship between σ^2 and Z . Figure 3 shows that the behaviors of σ^2 and Z given by equations (13) and (14) are very similar except for some particular DSDs. In order to limit the mentioned bias, we established three selection criteria on the DSDs.

[41] A first criterion on DSDs is based on rain rate consistency. In all DSDs, R appears as an input parameter, say R_{in} . However R can also be estimated by simply integrating the DSD through the well known relationship [*Meneghini and Kozu*, 1990]:

$$R_{estim} = 0.6\pi 10^{-3} \int_0^\infty N(D, R_{in}) D^3 v(D) dD \quad (22)$$

Table 1. Raindrop Size Distributions Used in This Study^a

Z	Type	N_0	DSR	Comments	Reference ^b
1	K	MP	$\Lambda = 4.1 R^{-0.21}$	Dyed filter paper	Marshall and Palmer [1948]
2	K	MP	$\Lambda = 3.0 R^{-0.21}$	IDS and radar, thunder	Joss et al. [1968]*
3	K	MP	$\Lambda = 5.7 R^{-0.21}$	IDS and radar, drizzle	Joss et al. [1968]*
4	K	g $\Gamma(0)$	$\Lambda = 3.8 R^{-0.14}$	Thunderstorm, Doppler radar	Sekhon and Srivastava [1971]*
5	N	g $\Gamma(0)$	$\Lambda = 3.52 R^{-0.23}$	Radar attenuation	Moupfouma and Tiffon [1982]*
6	M	g $\Gamma(0)$	$\Lambda = 5.11 R^{-0.253}$	Multiple frequency radar, R < 70 mm/h	Ihara et al. [1984]*
7	E	g $\Gamma(0)$	$\Lambda = 3.8 R^{-0.21}$	IDS	Wickers [1982]*
8	F	g $\Gamma(2)$	$\Lambda = 10 R^{-0.3}$	Radar attenuation, Mie, spherical drops	Gibbins [1992]*
9	P	g $\Gamma(2)$	$\Lambda = 145.16 R^{0.165}$	Radar attenuation, Mie, spherical drops	Li et al. [1994]
10	N	g $\Gamma(2)$	$\Lambda = 16.95 R^{0.037}$	Radar attenuation, Mie, spherical drops	Li et al. [1994]
11	P	g $\Gamma(3)$	$\Lambda = 5.753 R^{0.032}$	ODS and radar	Kozu et al. [2001]
12	N	I(6)	$b = 0.14 R^{0.34}$	ODS, gradient method R < 150 mm/h	Montanari [1997]
13	K	I(6)	$b = 0.13 R^{0.31}$	ODS, gradient method R < 150 mm/h	Montanari [1997]
14	E	I(8)	$b = 1.09 R^{0.13}/c$	300 m link, Mie, momentum method	Gloaguen and Lavergnat [1995]*
15	K	LN	$\mu = -0.33 + 0.166 \ln(R)$	ODS, momentum method R < 150 mm/h	Montanari [1997]
16	P	LN	$\mu = -0.309 + 0.134 \ln(R)$	ODS, momentum method R < 150 mm/h	Montanari [1997]
17	L	LN	$\mu = -0.195 + 0.199 \ln(R)$	IDS and radar	Ajayi and Olsen [1985]*
18	N	LN	$\mu = -0.0231 + 0.116 \ln(R)$	IDS and radar, 70 < R < 120 mm/h	Maciel and Assis [1990]
19	P	LN	$\mu = -0.4102 + 0.203 \ln(R)$	IDS and radar	Tharek and Din [1990]*
20	F	LN	$\mu = -0.133 + 0.127 \ln(R)$	IDS and radar, showers 5 < R < 50 mm/h, Data fitted by Ajayi and Olsen [1985]	Barclay et al. [1978]*
21	F	LN	$\mu = -0.451 + 0.264 \ln(R)$	IDS and radar, thunderstorm 5 < R < 50 mm/h	Barclay et al. [1978]*
22	F	LN	$\mu = 0.567$	IDS and radar, thunderstorm 5 < R < 200 mm/h	Barclay et al. [1978]*
23	P	LN	$\mu = -0.429 + 0.146 \ln(R)$	IDS	Ong and Shan [1997]*
24	P	LN	$\mu = -0.313 + 0.227 \ln(R)$	IDS and radar, stratiform rain R < 20 mm/h	Timothy et al. [2002]
25	P	LN	$\mu = -0.312 + 0.118 \ln(R)$	IDS and radar, convective rain R < 250 mm/h	Timothy et al. [2002]
26	W		$b = 0.26 R^{0.44}$	Drizzle, shower, radar attenuation	Sekin et al. [1987]*

^aNotes: Z, ITU-R rain climatic zones; MP, Marshall Palmer; g $\Gamma(g)$, generalized Gamma function of order g; $\Gamma(n)$, Gamma function with n parameters; LN, lognormal function; W, Weibull distribution; IDS, impact distrometer; ODS, optical distrometer.

^bReferences marked with an asterisk are recited from Montanari's [1997] compilation.

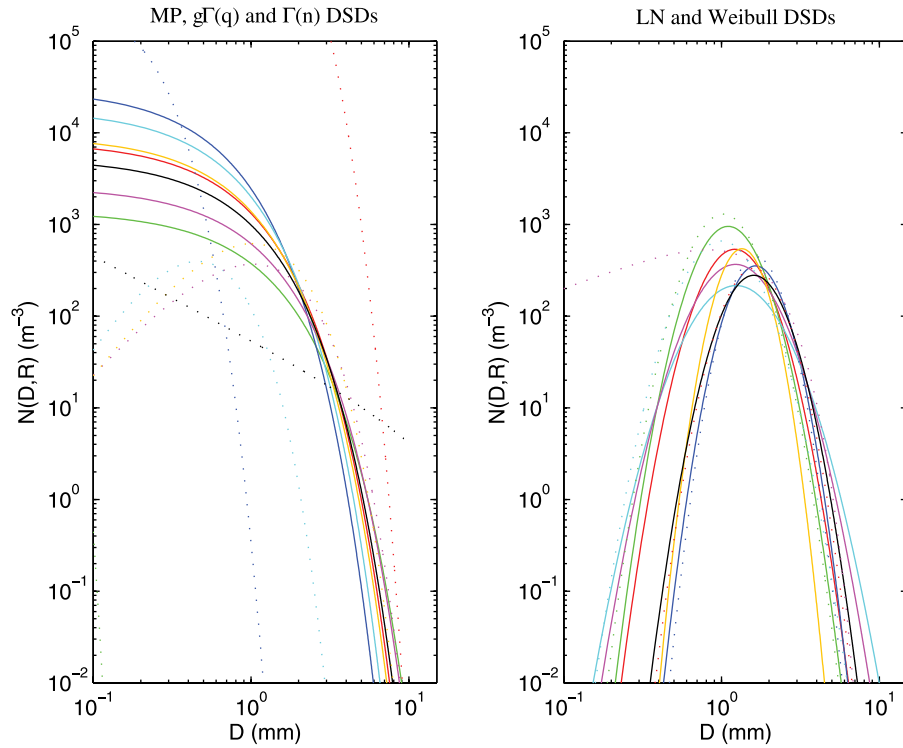


Figure 2. Drop size distributions under study for $R = 50 \text{ mm/h}$. Lines and colors refer to the first column in Table 1 as follows: (left) models 1–14, with continuous lines from 1 to 7, and dotted lines from 8 to 14; (right) models 15–26, with continuous lines from 15 to 21, and dotted lines from 22 to 26.

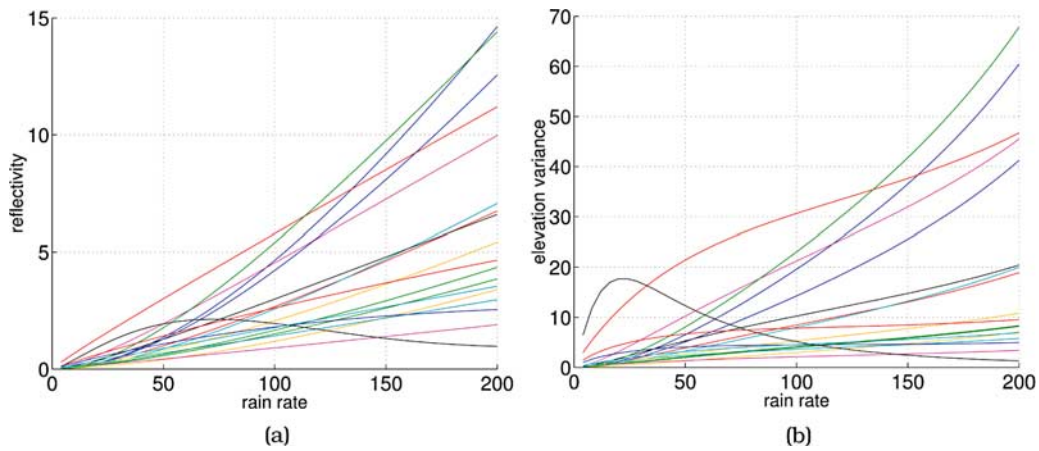


Figure 3. (a) Reflectivity at 13.8 GHz and (b) surface elevation variance obtained for the first 18 DSDs from Table 1 versus rain rate.

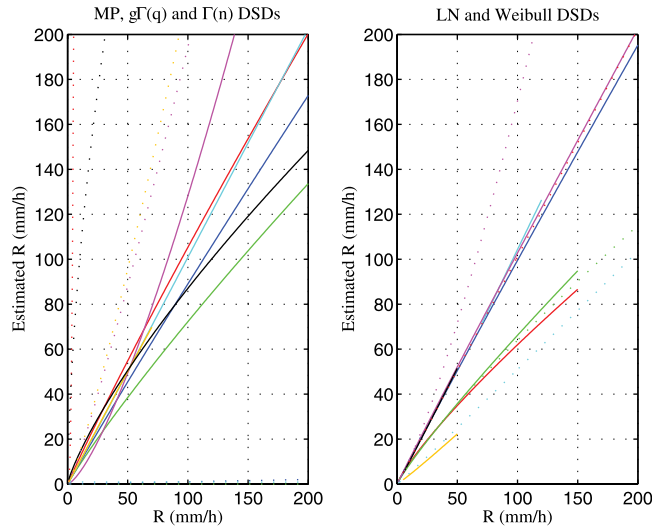


Figure 4. Estimated rain rate R_{estim} versus R_{in} for the DSD types from Table 1.

[42] In an ideal case R_{estim} and R_{in} should be equal. This is actually not the case as can be seen in Figure 4 that displays the estimated recalculated rain rate for the DSDs classified as in Figure 2. The discrepancies between R_{estim} and R_{in} may be used as a first selection criterion on the DSDs. Here we have chosen a three-step “acceptance” criterion based on calculations at $R_{in} = 100$ mm/h with relative errors on R_{in} not exceeding 10% (class I), 50% (class II), 100% (class III) or more (DSD rejected).

[43] A second criterion we chose is based on attenuation consistency, since this quantity is of great impor-

tance in rain radar retrieval algorithms. Similarly to rain rate consistency, we apply classical Mie calculation assuming spherical shapes in order to evaluate the extinction cross section σ_t of individual drops, then the specific attenuation k for all the DSDs under study by:

$$k = 4.343 \cdot 10^{-3} \int_0^\infty \sigma_t(D) N(D, R_{in}) dD \quad (23)$$

[44] Figure 5 shows the behavior of k versus R_{in} at 35 GHz for the DSD models highlighted in Figure 2.

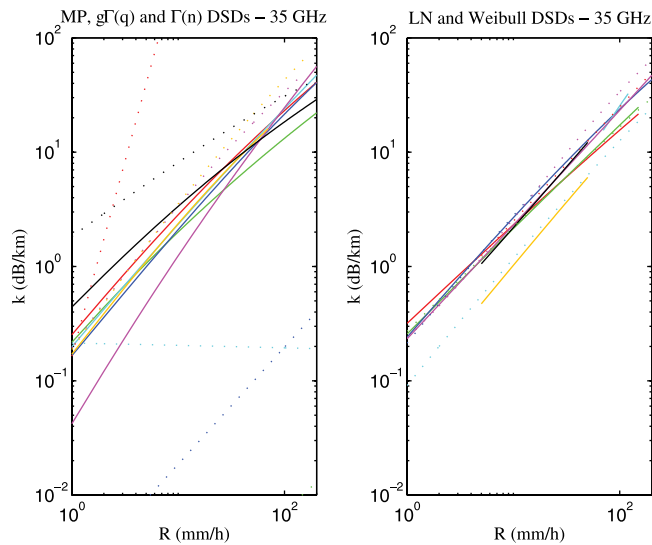


Figure 5. Specific attenuation k at 35 GHz versus rain rate R_{in} for the DSD types from Table 1.

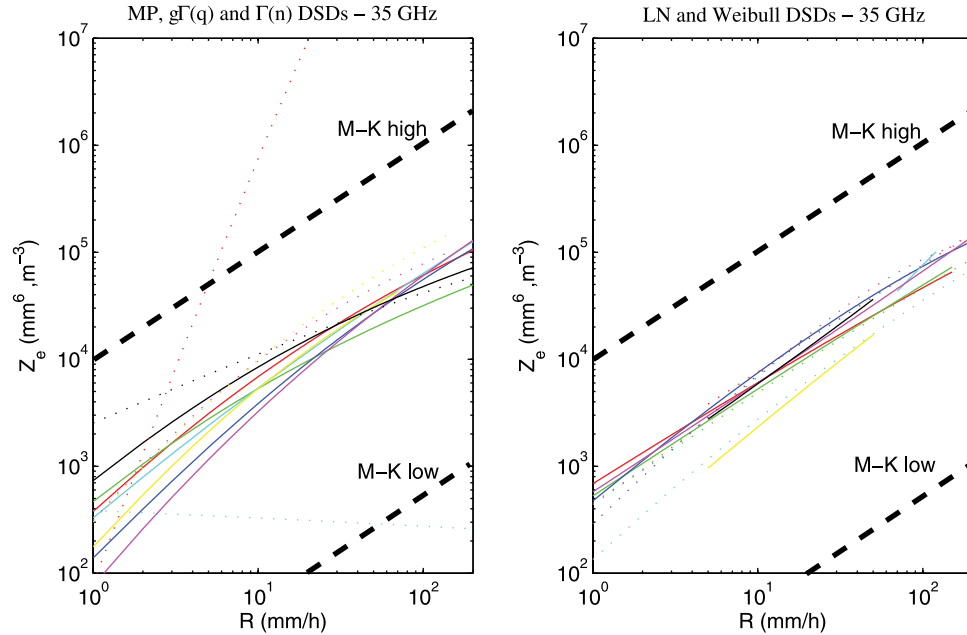


Figure 6. Rain radar reflectivities at 35 GHz versus rain rate for the DSD types from Table 1. M-K high and M-K low lines indicate upper and lower limits from *Meneghini and Kozi* [1990, Figure 4.9] for several $Z - R$ relationships.

Similar calculations have been performed for various frequencies between 3 and 94 GHz. Again it appears that some of the specific attenuation curves clearly depart from the general trend, and that some of these can certainly be questioned because they yield very large differences with respect to the typical values that may be found in literature [*Meneghini and Kozi*, 1990].

[45] A similar Mie type calculation has been made on spherical raindrops in order to evaluate their backscattering cross section σ_b . It has then been integrated to get the rain reflectivity versus rain rate R_m too. An example of this calculated reflectivity, denoted hereafter by Z_e , is shown for 35 GHz in Figure 6. To check their validity, the previous calculations have been compared with other reflectivity models available in the literature as, for instance, those in the work of *Meneghini and Kozi* [1990]. In Figure 6 in addition to data points calculated in this paper, the upper and lower limits entitled “M-K high” and “M-K low” that can be found as upper and lower limits in Figure 4.9 of *Meneghini and Kozi* [1990] are reproduced and indicate the consistency of our calculations.

[46] Combining those criteria we have constructed three sets of acceptable DSDs depending on an increasing relative error on the recalculated rain rate, as mentioned above, and yielding reasonable attenuation and

rain radar reflectivity ranges. We have discarded the other ones.

[47] Three successive steps were then considered for the evaluation of the $\sigma^2(Z_e)$ relationship searched for: first, with the more strict criteria in the first one (step I), then relaxing them in steps II and III, as will be shown in the next section. Table 2 shows the DSDs from Table 1 reorganized into four classes: the three accepted classes and the rejected one.

6. Rain-Induced Surface Variance Versus Rain Radar Reflectivity

[48] The similarity of the integrals appearing in the expressions of the elevation variance (13) and of the reflectivity factor (14) has already been pointed out. Hence, those two quantities, even if not proportional to each other, will have similar behaviors. In other terms, the relationship between rain reflectivity and elevation variance is expected to present a rather weak dependence on the actual model chosen for the DSD.

[49] Most of the rain radar retrieval algorithms make use of power law relationships between each pair of the three quantities R , k and Z . This choice will not be criticized here and a similar formulation will be searched.

Table 2. Selection Results of DSDs Under Study With Parameters Calculated at 35 GHz

Class	DSD	Type	Error (%)	k_{\min} (dB)	k_{\max} (dB)	$Z_{e1\text{mm/h}} \cdot 10^3$ (mm ⁶ /m ³)	$Z_{e200\text{mm/h}} \cdot 10^5$ (mm ⁶ /m ³)
I	1	MP	5	0.25	40.81	3.78	10.40
I	4	$g\Gamma(0)$	1	0.20	47.13	4.67	4.94
I	6	$g\Gamma(0)$	1	0.17	38.92	1.39	10.79
I	17	LN	0	0.24	43.17	3.30	12.54
I	18	LN	4	0.03	60.30	0.77	12.92
I	19	LN	3	0.23	47.05	1.77	9.89
I	21	LN	5	0.19	56.46	7.35	7.17
I	22	LN	1	0.25	49.85	0.80	$1.4 \cdot 10^{-6}$
I	24	LN	5	0.21	45.34	$6.0 \cdot 10^{-8}$	$3.0 \cdot 10^{-8}$
II	2	MP	28	0.22	22.08	$2.6 \cdot 10^{-3}$	$3.7 \cdot 10^{-3}$
II	3	MP	11	0.17	40.65	2.60	0.04
II	5	$g\Gamma(0)$	28	0.04	56.23	3.13	12.57
II	7	$g\Gamma(0)$	13	0.44	28.87	3.01	19.45
II	15	LN	38	0.32	27.14	25.41	5.81
II	16	LN	34	0.26	31.95	6.88	8.27
II	23	LN	36	0.27	29.87	5.28	9.51
II	25	LN	49	0.09	24.69	4.74	12.72
III	12	$\Gamma(6)$	94	0.19	62.04	0.48	18.71
III	20	LN	53	0.08	26.49	5.76	14.06
III	26	W	70	0.24	64.99	1.16	8.36
rejected	8	$g\Gamma(2)$	$2.8 \cdot 10^6$	0.16	$5.1 \cdot 10^6$	4.83	20.17
rejected	9	$g\Gamma(2)$	100	$1.9 \cdot 10^{-4}$	0.01	7.61	15.23
rejected	10	$g\Gamma(2)$	99	$1.8 \cdot 10^{-3}$	0.40	4.38	8.70
rejected	11	$g\Gamma(3)$	99	0.21	0.19	2.89	13.30
rejected	13	$\Gamma(6)$	118	0.19	84.87	1.34	7.01
rejected	14	$\Gamma(8)$	284	1.83	43.14	4.52	13.20

Therefore for the selected DSDs, both $\sigma^2(R)$ and $Z_e(R)$ (not converted in dBZ) have been computed for $0 < R < 200$ mm/h. This allowed us to obtain (σ^2, Z_e) pairs for each DSD, at different frequencies, rain rates and classes. Then, we performed first- and second-order polynomial identifications between σ^2 and Z_e in the logarithmic domain:

$$\log(\sigma^2) = p_{1a} \log Z_e + p_{1b} \quad (24)$$

$$\log(\sigma^2) = p_{2a} (\log Z_e)^2 + p_{2b} \log Z_e + p_{2c} \quad (25)$$

where the first-order (p_{1a} and p_{1b}) and second-order polynomial coefficients (p_{2a} , p_{2b} and p_{2c}) are determined in a least squares sense.

[50] Figures 7, 8, and 9 show the scatterplots and the first-order and second-order regression curves at 3, 13.8, and 35 GHz for the three classes specified in Table 2.

[51] Table 3 gives the numerical values of the first- and second-order coefficients of the polynomials, for seven frequencies between 3 and 94 GHz for each DSD class. Table 4 shows the corresponding mean error estimates for confidence intervals of 50%, 90%, and 95%, respectively. From Table 4 we observe that the chosen models approximate the simulated data well and that the second-

order polynomials are more accurate than the first-order ones to derive a law for the $\sigma^2(Z_e)$ relationship, even though the gain in accuracy is significant for small values of σ^2 and Z_e only. Third-order polynomials were also tested, but no significant gain was found in comparison with the already obtained regressions.

[52] These fits have also been analyzed versus frequency. Figure 10 shows a comparison of all second-order polynomials, whose coefficients are given in Table 3. In Figure 10 we observe that the fits are quite close to each other for all frequencies below 14 GHz, and that for the fit at 35 GHz the deviation increases, while for 94 GHz the curves depart strongly from the other ones. This is not surprising because at such a high frequency the scattering of hydrometeors strongly departs from the D^6 dependence used as an approximate basis for this study. In other words, when in terms of wavelength the largest drops leave the Rayleigh region to the resonance region, σ^2 and Z_e no longer represent similar moments of the DSD and the latter will bring little information on the former. This is certainly what happens for frequencies beyond 40 GHz. It should also be underlined that for class I the second-order term appears nonnegligible, while extending the DSD class size from I to III, the dependence becomes more linear in the log-log domain. This means that the inclusion of

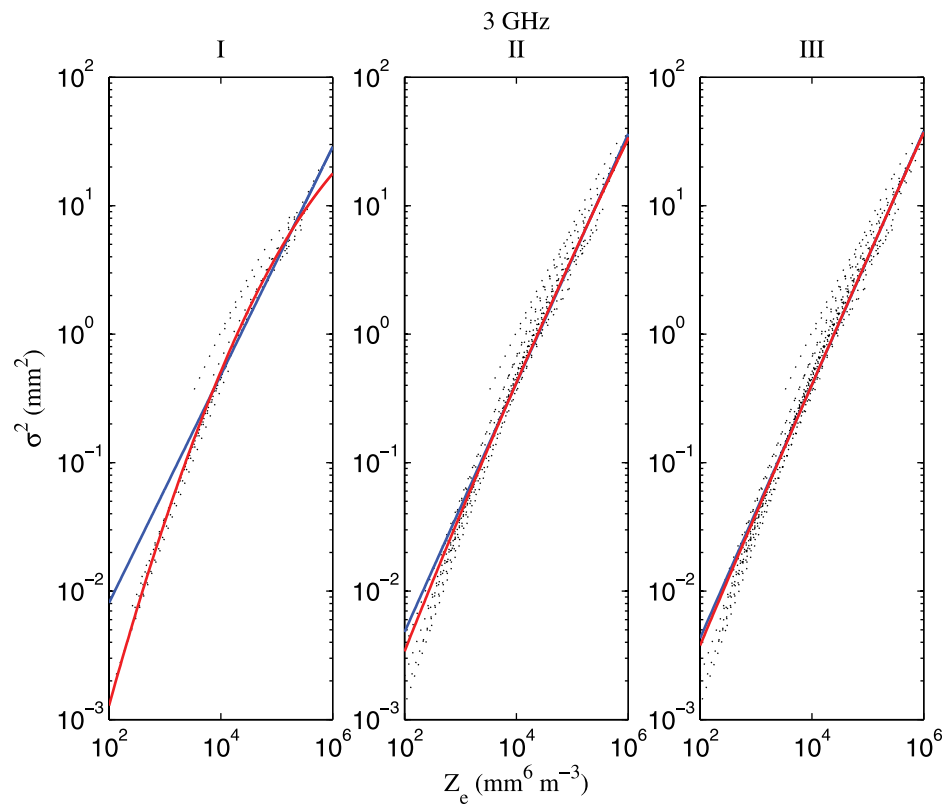


Figure 7. The σ^2 - Z_e first-order (blue lines) and second-order (red lines) logarithmic polynomial fitting at 3 GHz for the three classes of selected DSDs (dotted lines) from Table 2, class I, II or III, respectively.

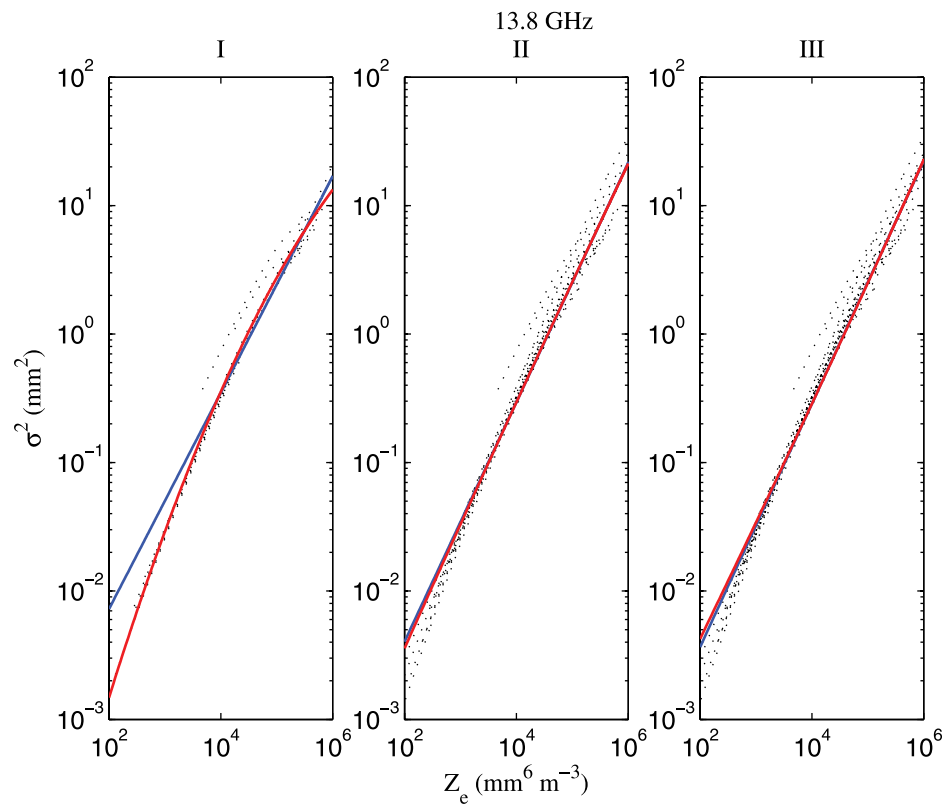


Figure 8. The σ^2 - Z_e first-order (blue lines) and second-order (red lines) logarithmic polynomial fitting at 13.8 GHz for the three classes of selected DSDs (dotted lines) from Table 2, class I, II or III, respectively.

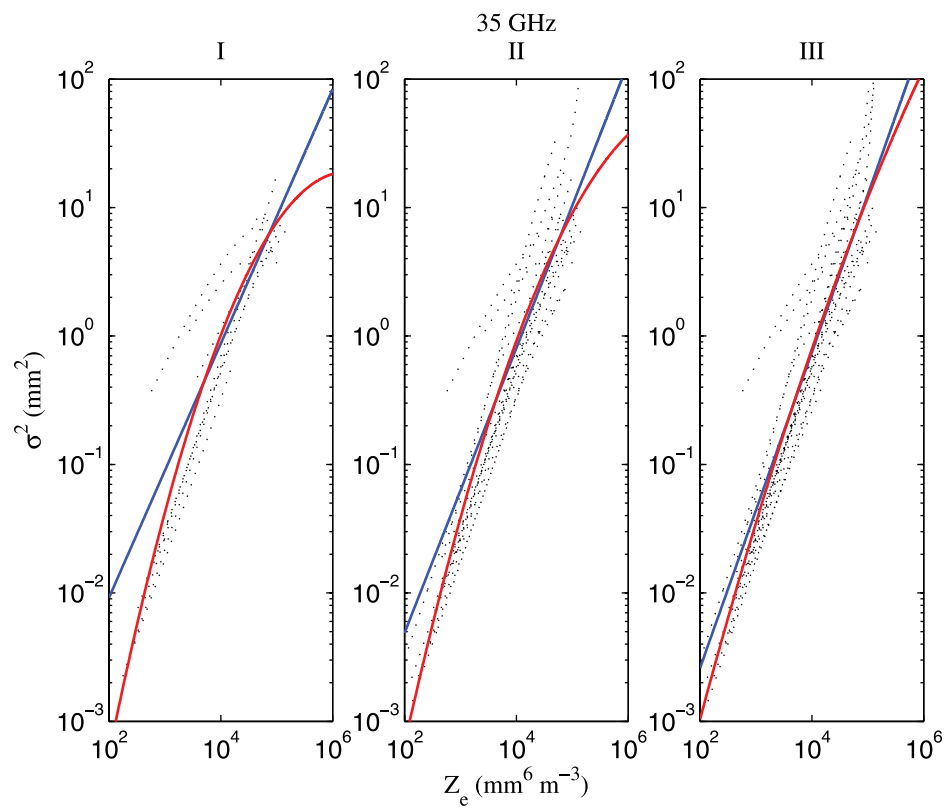


Figure 9. The σ^2 – Z_e first-order (blue lines) and second-order (red lines) logarithmic polynomial fitting at 35 GHz for the three classes of selected DSDs (dotted lines) from Table 2, class I, II or III, respectively.

Table 3. The σ^2-Z_e Polynomial Fitting Coefficients for the Classes of Selected DSDs

Frequency, GHz	Step	First Order		Second Order		
		p_{1a}	p_{1b}	p_{2a}	p_{2b}	p_{2c}
3	I	0.8875	-3.8676	-0.1325	2.0951	-6.5522
	II	0.9691	-4.2575	-0.0237	1.1880	-4.7507
	III	0.9862	-4.3387	-0.0085	1.0655	-4.5203
5.3	I	0.8725	-3.8026	-0.1291	2.0571	-6.4541
	II	0.8808	-3.8586	-0.0686	1.5342	-5.3791
	III	0.8966	-3.9341	-0.0546	1.4245	-5.1770
10	I	0.8217	-3.6955	-0.0992	1.7540	-5.8244
	II	0.8746	-3.9511	-0.0307	1.1686	-4.6378
	III	0.8837	-3.9957	-0.0169	1.0483	-4.3859
13.8	I	0.8423	-3.8257	-0.1014	1.7995	-6.0240
	II	0.9319	-4.2590	-0.0074	1.0018	-4.4210
	III	0.9468	-4.3307	0.0087	0.8632	-4.1341
24	I	0.9095	-3.9936	-0.1681	2.4514	-7.4530
	II	1.0581	-4.6860	-0.0352	1.3764	-5.3902
	III	1.1188	-4.9693	0.0271	0.8711	-4.4157
35	I	0.9893	-4.0161	-0.2505	3.1322	-8.5158
	II	1.1093	-4.5313	-0.1917	2.7200	-7.8524
	III	1.2287	-5.0421	-0.0873	1.9641	-6.5614
94	I	0.8902	-1.8699	-0.4103	3.0267	-4.5890
	II	1.0189	-2.2667	-0.6522	4.4120	-6.5918
	III	1.2017	-2.7149	-0.7560	5.1211	-7.6935

Table 4. Error Estimate Mean Values for the Fits at Different Frequencies and Confidence Intervals

Frequency, GHz	Step	50%		90%		95%	
		First	Second	First	Second	First	Second
3	I	0.0754	0.0607	0.1840	0.1480	0.2193	0.1764
	II	0.0823	0.0818	0.2007	0.1995	0.2392	0.2377
	III	0.0814	0.0814	0.1986	0.1985	0.2366	0.2365
5.3	I	0.0583	0.0337	0.1422	0.0823	0.1695	0.0981
	II	0.0612	0.0492	0.1492	0.1201	0.1778	0.1431
	III	0.0666	0.0588	0.1625	0.1434	0.1936	0.1709
10	I	0.0564	0.0392	0.1375	0.0956	0.1639	0.1140
	II	0.0576	0.0554	0.1406	0.1352	0.1676	0.1611
	III	0.0594	0.0586	0.1449	0.1430	0.1727	0.1704
13.8	I	0.0721	0.0606	0.1759	0.1479	0.2097	0.1762
	II	0.0842	0.0842	0.2054	0.2055	0.2448	0.2448
	III	0.0835	0.0835	0.2037	0.2036	0.2428	0.2426
24	I	0.1206	0.1101	0.2941	0.2685	0.3506	0.3201
	II	0.1701	0.1702	0.4150	0.4151	0.4945	0.4947
	III	0.1701	0.1702	0.4149	0.4151	0.4944	0.4946
35	I	0.1577	0.1504	0.3849	0.3670	0.4587	0.4374
	II	0.2419	0.2399	0.5901	0.5852	0.7032	0.6974
	III	0.2525	0.2537	0.6159	0.6188	0.7340	0.7374
94	I	0.2611	0.2586	0.6370	0.6309	0.7592	0.7519
	II	0.3372	0.3283	0.8225	0.8009	0.9802	0.9544
	III	0.3589	0.3481	0.8755	0.8491	1.0433	1.0119

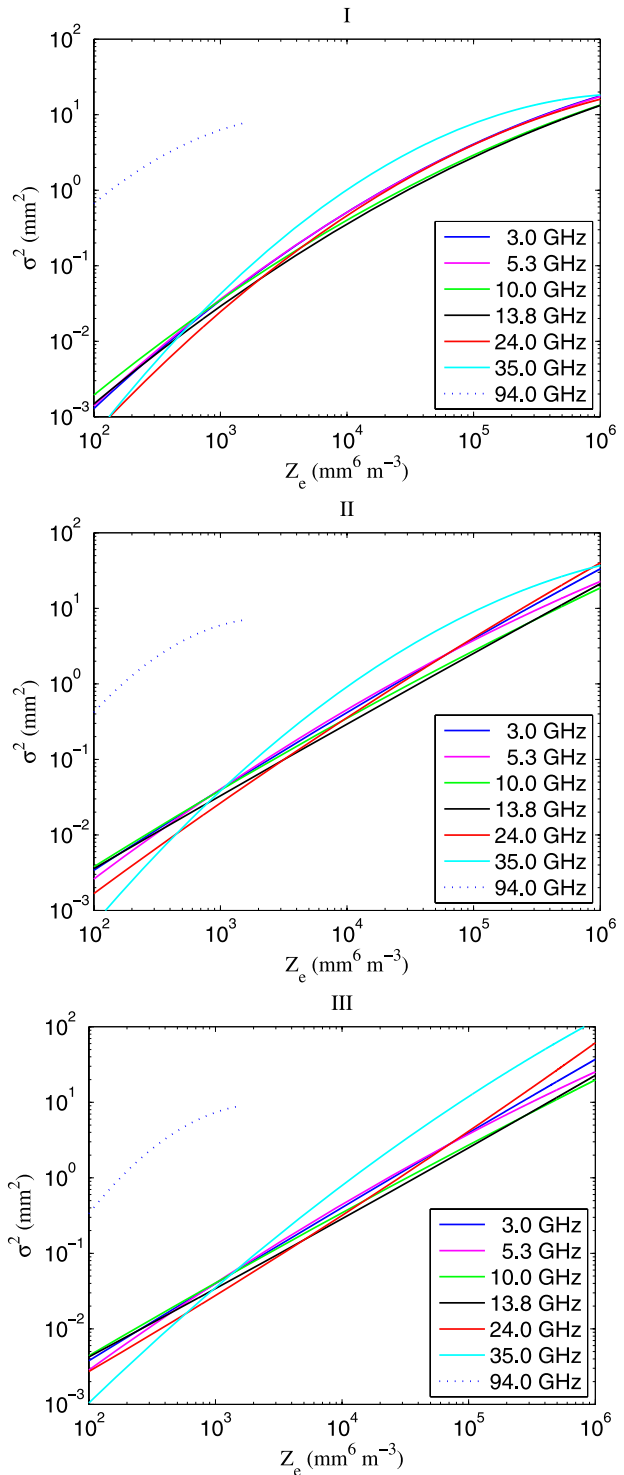


Figure 10. The σ^2-Z_e second-order logarithmic polynomial fitting for the three classes of selected DSDs and the different frequencies. Coefficients are from Table 3.

Table 5. Second-Order Polynomial Coefficients of σ^2-Z_e Over Different Frequency Bands, and Rayleigh Case^a

Frequency Band	Average Coefficients		
	p_{2a}	p_{2b}	p_{2c}
Rayleigh	-0.0184	1.1334	-4.6493
3–13.8 GHz	-0.0178	1.1004	-4.5543
3–24.0 GHz	-0.0128	1.0749	-4.5389
3–35.0 GHz	-0.0165	1.1274	-4.6696

^aClass III DSD.

DSDs from less strict classes, in the sense of our selection criteria, simultaneously decreases the significance of the second-order terms, along with an increase of the error interval.

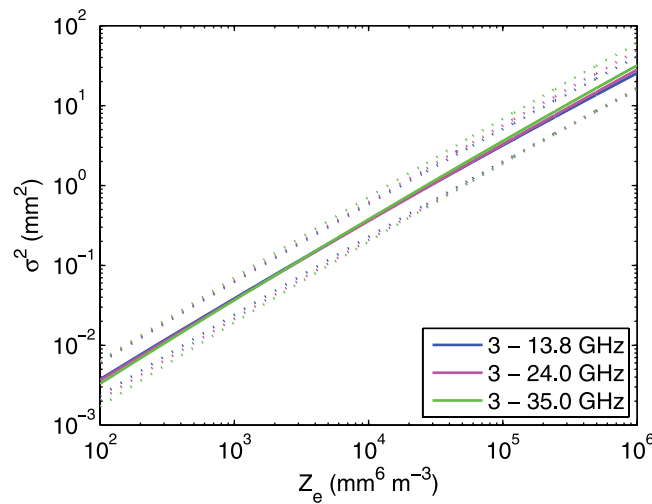
[53] For the sake of completeness, a comparison with non-Mie scattering has been conducted by repeating the complete procedure with the Rayleigh approximation. A global average fit combining the different frequencies in bands up to 35 GHz has also been made. The results of the corresponding second-order coefficients for class III are given in Table 5. The first-order coefficients close to unity and second-order coefficients relatively small illustrate the quasi-proportionality between σ^2 and Z_e that can be also observed on the corresponding Figure 11 in which 95% confidence intervals have been indicated also.

7. Discussion

[54] The dependence of σ^2 on D^6 highlighted here supports the fact that the surface roughness due to

impacting rain increases very fast with drop size. As a result, mostly the large drops affect this surface roughness. This effect is very difficult to estimate when only the rain rate is known, because the large drop content strongly depends on the models chosen for the DSD. It has been shown in this paper that this uncertainty can be reduced when drop reflectivity data Z are available, as it is the case for nadir looking spaceborne rain radar data. Indeed, drop reflectivity and surface elevation variance correspond to similar moments of the drop size distribution. Therefore the rain-induced surface variance σ^2 can be calculated from the Z estimated just above the surface following the proposed scheme.

[55] Further, the rain spectral component added to the wind spectral one can be estimated more accurately than using the rain rate only. The surface backscattering coefficient change $\Delta\sigma^\circ$ can then be calculated by using available electromagnetic models and codes, for the remote sensing geometries of interest, and introduced in rain radar algorithms for further improvement of rain rate retrievals. In Figure 12, an example for such a calculation of $\Delta\sigma^\circ$ at 13.8 GHz and 35 GHz is given for nadir incidence and for rain rates ranging from 0 to 100 mm/h. $\Delta\sigma^\circ$ is related to Z_e just above the surface through the $\sigma^2(Z_e)$ relationship proposed in this study. The conditions for this example are: DSD class I, fully developed sea state conditions with a wind friction velocity $u_* = 20$ cm/s (i.e., $U_{10} \simeq 6$ m/s wind at 10 m height) using the wind sea surface spectrum and electromagnetic scattering models from *Elfouhaily et al.* [1997] or *Lemaire et al.* [1999], respectively. The additive surface spectrum due to rain is taken from *Craeye* [1998]. The

**Figure 11.** Second-order polynomial fitting for σ^2-Z_e along with 95% confidence intervals over different frequency bands. Class III DSD.

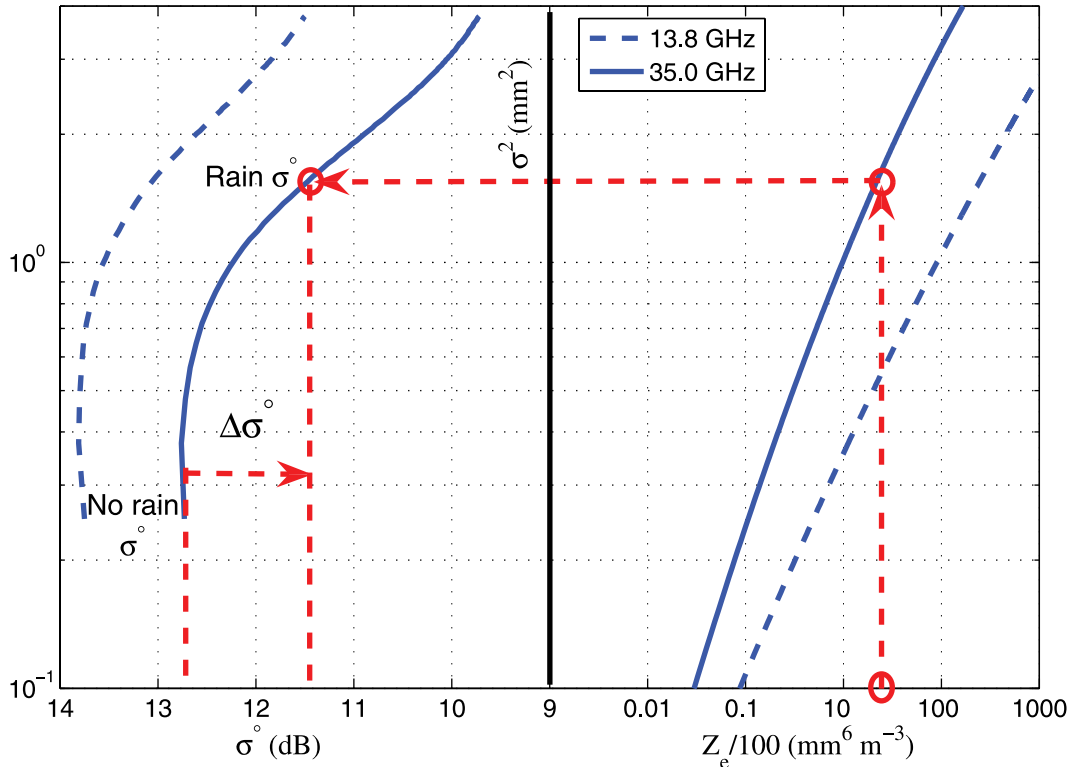


Figure 12. Sea surface backscattering coefficient change $\Delta\sigma^\circ$ at 13.8 GHz and 35 GHz, for nadir incidence and rain rates ranging from 0 to 100 mm/h, related to Z_e just above the surface through the $\sigma^2(Z_e)$ relationship proposed in this study and numerical models for σ° . Class I DSD, wind friction velocity $u_* = 20$ cm/s (wind $U_{10} \simeq 6$ m/s), wind sea surface spectrum and electromagnetic scattering models are from *Elfouhaily et al.* [1997] and *Lemaire et al.* [1999]; additive surface spectrum due to rain is from *Craeye* [1998].

arrows on Figure 12 indicate how a measurement of Z_e just above the surface can provide an estimate of σ^2 and, in turn, an evaluation of $\Delta\sigma^\circ$ with respect to σ° in the nonrainy case.

[56] In the example shown here, $\Delta\sigma^\circ$ is limited up to 1 to 2 dB for the range of the chosen conditions. It would be interesting to validate such a procedure against measured data. As direct $\Delta\sigma^\circ$ measurements at nadir noncontaminated by rain attenuation are very sparse, what is one motivation of this paper, an indirect approach to compare the range of $\Delta\sigma^\circ$ with measurements could be followed. Well-documented field radar data at Ku band for various incidence angles versus wind and rain are available in the work of *Contreras et al.* [2003]. Nadir $\Delta\sigma^\circ$ are not available. Analyzing the reported results and the evolution of σ° for decreasing incidence angles from 76 down to 14, we observe that the simulated σ° using this procedure for similar environmental conditions are consistent with the data, even though the sign of $\Delta\sigma^\circ$ (increase or decrease versus rain rate)

depends on the sea state conditions. Therefore more well documented data including sea state conditions for combined wind and rain are needed to further validate the radar backscattering by the surface at nadir or near nadir.

8. Conclusion

[57] A relationship between Z obtained from rain radars and ringwaves height variance σ^2 has been established. A possible procedure to derive $\Delta\sigma^\circ$ at nadir from Z data has been further suggested once an electromagnetic scattering model has been chosen. Further refinements are possible and could include nonspherical drop shapes, a large database of DSD, as well as iterative retrieval algorithms for both rain rate and surface variance.

[58] **Acknowledgments.** The authors thank Ana Rita Araujo for the detailed analysis of the DSD effect and anonymous reviewers for very helpful comments.

References

- Ajayi, G. O., and R. Olsen (1985), Modeling of a tropical rain-drop size distribution for microwave and millimeter waves applications, *Radio Sci.*, 20(2), 193–202.
- Alpers, W., and I. I. Lin (2006), Rain cells associated with atmospheric fronts over the ocean studied by spaceborne SAR and weather radar data, in *Proceedings of SEASAR 2006 Workshop (Advances in SAR Oceanography From Envisat and ERS Missions, Frascati, Italy)*, ESA Spec. Publ. SP-613, Publ. Div., Eur. Space Agency, Noordwijk, Netherlands.
- Atlas, D. (1994), Footprints of storms on the sea: A view from spaceborne synthetic aperture radar, *J. Geophys. Res.*, 99(C4), 7961–7969.
- Barclay, P. A., J. A. Bennett, and R. C. Boston (1978), Properties of rain for microwave propagation studies, *Rep. MEE-78-1*, pp. 35–68, Electr. Eng. Dep., Monash Univ., Melbourne, Victoria, Australia.
- Black, P. G., R. C. Gentry, V. J. Cardone, and J. D. Hawkins (1985), Seasat microwave wind and rain observations in severe tropical and midlatitude marine storms, *Adv. Geophys.*, 27, 198–278.
- Bliven, F. L., H. Branger, P. Sobieski, and J.-P. Giovanangeli (1993), An analysis of scatterometer returns from a water surface agitated by artificial rain: evidence that ringwaves are the main feature, *Int. J. Remote Sens.*, 14, 2315–2329.
- Bliven, F. L., P. Sobieski, and C. Craeye (1997), Rain generated ringwaves: Measurements and modeling for remote sensing, *Int. J. Remote Sens.*, 18, 221–228.
- Braun, N., and M. Gade (2006), Multi-frequency scatterometer measurements on water surfaces agitated by artificial and natural rain, *Int. J. Remote Sens.*, 27(1), 27–39.
- Braun, N., M. Gade, and P. A. Lange (2002), The effect of artificial rain on wave spectra and multi-polarisation X band radar backscatter, *Int. J. Remote Sens.*, 23(20), 4305–4323.
- Contreras, R. F., and W. J. Plant (2004), Ku-band backscatter from the Cowlitz River: Bragg scattering with and without rain, *IEEE Trans. Geosci. Remote Sens.*, 42(7), 1444–1449.
- Contreras, R. F., and W. J. Plant (2006), Surface effect of rain on microwave backscatter from the ocean: Measurements and modeling, *J. Geophys. Res.*, 111, C08019, doi:10.1029/2005JC003356.
- Contreras, R. F., W. J. Plant, W. C. Keller, K. Hayes, and J. A. Nuysten (2003), Effects of rain on Ku band backscatter from the ocean, *J. Geophys. Res.*, 108(C5), 3165, doi:10.1029/2001JC001255.
- Craeye, C. (1998), Radar signatures of the sea surface perturbed by rain, Ph.D. thesis, Univ. cath. de Louvain, Louvain-la-Neuve, Belgium. (Available at <http://www.tele.ucl.ac.be>)
- Craeye, C., P. Sobieski, and F. L. Bliven (1997), Scattering by artificial wind and rain roughened water surfaces at oblique incidences, *Int. J. Remote Sens.*, 18(10), 2241–2246.
- Craeye, C., P. Sobieski, L. F. Bliven, and A. Guissard (1999), Ring-waves generated by water drops impacting on water surfaces at rest, *IEEE Trans. Oceanic Eng.*, 24(3), 323–332.
- Draper, D. W., and D. G. Long (2004a), Simultaneous wind and rain retrieval using SeaWinds data, *IEEE Trans. Geosci. Remote Sens.*, 42(7), 1411–1423.
- Draper, D. W., and D. G. Long (2004b), Assessing the quality of SeaWinds rain measurements, *IEEE Trans. Geosci. Remote Sens.*, 42(7), 1424–1432.
- Durden, S. L., L. Li, E. Im, and S. H. Yueh (2003), A surface reference technique for airborne Doppler radar measurements in hurricanes, *J. Atmos. Oceanic Technol.*, 20(2), 269–275.
- Elfouhaily, T. M., B. Chapron, K. Katsaros, and D. Vandemark (1997), A unified directional spectrum for long and short wind-driven waves, *J. Geophys. Res.*, 102(C7), 15,781–15,796.
- Ferreira, F., P. Amayenc, S. Oury, and J. Testud (2001), Study and tests of improved rain estimates from the TRMM precipitation radar, *J. Appl. Meteorol.*, 40(11), 1878–1899.
- Gibbins, C. J. (1992), Studies of millimetre-wave propagation and related meteorology over a 500 m path, in *Proceedings of Commission F Open Symposium*, Int. Union of Radio Sci., Ghent, Belgium.
- Gloaguen, C., and J. Lavernat (1995), Raindrop size distribution near Paris, *IEE Electron. Lett.*, 31(5), 405–406.
- Gunn, K. L. S., and G. D. Kinzer (1949), The terminal velocity of fall for water droplets in stagnant air, *J. Meteorol.*, 6, 243–248.
- Guymet, T. H., J. A. Businger, and W. L. Jones (1981), Anomalous wind estimates from the Seasat scatterometer, *Nature*, 294, 735–737.
- Haddad, Z. S., D. A. Short, S. L. Durden, I. Eeastwood, S. Hensley, M. B. Grable, and R. A. Black (2004), A new parametrization of the raindrop size distribution, *IEEE Trans. Geosci. Remote Sens.*, 35(3), 532–539.
- Hallett, J., and L. Christensen (1984), Splash and penetration of drops in water, *J. Rech. Atmos.*, 18, 225–242.
- Hansen, J. P. (1986), Rain backscatter tests dispel old theories, *Microwaves RF J.*, 97–98, 101–102.
- Hendrantoro, G., and I. Zawadzki (2003), Derivation of parameters of y-z power law relation from raindrop size distribution measurements and its application in the calculation of rain attenuation from radar reflectivity factor measurements, *IEEE Trans. Antennas Propag.*, 51(1), 12–22.
- Hitschfeld, W., and J. Bordan (1954), Errors inherent in the radar measurement of rainfall at attenuating wavelengths, *J. Meteorol.*, 11, 58–67.
- Iguchi, T., T. Kozu, R. Meneghini, J. Awaka, and K.-I. Okamoto (2000), Rain-profiling algorithm for the TRMM precipitation radar, *J. Appl. Meteorol.*, 39(12, Part 1), 2038–2052.
- Ihara, T., Y. Furuhashi, and T. Manabe (1984), Inference of raindrop size distribution from rain attenuation statistics at 12, 35 and 82 GHz, *Trans. IECE Jpn.*, E67(4), 211–217.
- Joss, J., J. C. Thams, and A. Waldvogel (1968), The variation of raindrop size distributions at Locarno, in *Proceedings of International Conference on Cloud Physics*, pp. 369–373,

- Int. Assoc. of Meteorol. and Atmos. Phys., Toronto, Ont., Canada.
- Kozu, T., K. Nakamura, R. Meneghini, and W. C. Bonczyk (1991), Dual-parameter radar rainfall measurement from space: A test results from an aircraft experiment, *IEEE Trans. Geosci. Remote Sens.*, 29, 690–703.
- Kozu, T., K. K. Reddy, A. R. Jain, T. Shimomai, and K. Ichikawa (2001), Seasonal variation of raindrop size distribution in south India obtained from disdrometer measurements supported by wind-profiler measurements, in *Proceedings of 30th International Conference on Radar Meteorology, Munich, Germany*, Am. Meteorol. Soc., Boston, Mass.
- Lemaire, D., P. Sobieski, and A. Guissard (1999), Full-range sea surface spectrum in non-fully developed state for scattering calculations, *IEEE Trans. Geosci. Remote Sens.*, 37(2), 1038–1051.
- Lemaire, D., L. F. Bliven, C. Craeye, and P. Sobieski (2002), Drop size effects on rain-generated ringwaves with a view to remote sensing applications, *Int. J. Remote Sens.*, 23, 2345–2357.
- Le Méhauté, B. (1988), Gravity-capillary rings generated by water drops, *J. Fluid Mech.*, 197, 415–427.
- Le Méhauté, B., S. Wang, and C. C. Lu (1987), Spikes, domes and cavities, *J. Int. Assoc. Hydraul. Res.*, 5, 583–602.
- Li, L. W., P. S. Kooi, M. S. Leong, and T. S. Yeo (1994), A Gamma distribution of raindrop sizes and its applications to Singapore's tropical environment, *Microwave Opt. Technol. Lett.*, 7(5), 253–257.
- Maciel, L., and M. Assis (1990), Tropical rainfall drop-size distribution, *Int. J. Satell. Commun.*, 8, 181–186.
- Manton, M. (1973), On the attenuation of sea waves by rain, *Geophys. Fluid Dyn.*, 5, 249–260.
- Marshall, J. S., and W. M. Palmer (1948), The distribution of raindrops with size, *J. Meteorol.*, 5, 165–166.
- Melsheimer, C., W. Alpers, and M. Gade (2001), Simultaneous observations of rain cells over the ocean by the synthetic aperture radar aboard the ERS satellites and by surface-based weather radars, *J. Geophys. Res.*, 106, 4556–4677.
- Meneghini, R., and T. Kozu (1990), *Spaceborne Weather Radar*, Aertech House, Norwood, Mass.
- Meneghini, R., and L. Liao (2007), Tests of spaceborne rain retrieval algorithms using airborne radar data, in *Proceedings of International Geoscience and Remote Sensing Symposium (IGARSS'07), Barcelona, Spain*, IEEE Press, Piscataway, N. J.
- Meneghini, R., T. Kozu, H. Kumagai, and W. C. Bonczyk (1992), A study of rain estimation methods from space using dual-wavelength radar measurements at near-nadir over ocean, *J. Atmos. Oceanic Technol.*, 9, 364–382.
- Meneghini, R., T. Iguchi, T. Kozu, L. Liao, K. Okamoto, J. A. Jones, and J. Kwiatkowski (2001), Use of the surface reference technique for path attenuation estimates from the TRMM precipitation radar, *J. Appl. Meteorol.*, 39(12), 2053–2070.
- Montanari, C. (1997), The raindrop size distribution and applications to scattering and extinction, Ph.D. thesis, 178 pp., Univ. of Portsmouth, Portsmouth, U. K.
- Moore, R. K., Y. S. Yu, A. K. Fung, D. Kaneko, G. J. Dome, and R. E. Werp (1979), Preliminary study of rain effects on radar scattering from water surfaces, *IEEE J. Oceanic Eng.*, OE-4(1), 31–32.
- Moupfouma, F., and J. Tiffon (1982), Raindrop size distribution from microwave scattering measurements in equatorial and tropical climates, *IEE Electron. Lett.*, 18(23), 1012–1014.
- Nakamura, K., and T. Iguchi (2007), Dual-wavelength radar algorithm, in *Measuring Precipitation From Space, Adv. Global Change Res.*, vol. 28, pp. 225–234, doi:10.1007/978-1-4020-5835-6, Springer, New York.
- Nuysten, J. A. (1990), A note on the attenuation of surface gravity waves by rainfall, *J. Geophys. Res.*, 95(C10), 18,353–18,355.
- Ong, J. T., and Y. Y. Shan (1997), Raindrop size distribution models for Singapore-comparison with results from different regions, *Proc. Int. Conf. Antennas Propag.*, 436(2), 281–285.
- Rein, M. (1993), Phenomena of liquid drop impact on solid and liquid surface, *Fluid Dyn. Res.*, 12, 61–93.
- Reynolds, O. (1900), On the action of rain calming the sea, in *Papers on Mechanical and Physical Subjects*, vol. 1, pp. 86–88, Cambridge Univ. Press, New York.
- Sekhon, R. S., and R. C. Srivastava (1971), Doppler radar observation of drop-size distribution in a thunderstorm, *J. Atmos. Sci.*, 28(24), 983–994.
- Sekin, M., C. Chen, and T. Mush (1987), Rain attenuation from log-normal and Weibull raindrop size distributions, *IEEE Trans. Antennas Propag.*, 35, 358–359.
- Sobieski, P., and F. L. Bliven (1995), Scatterometry of a drop impact on a salt water surface, *Int. J. Remote Sens.*, 16(14), 2721–2726.
- Sobieski, P., C. Craeye, and L. F. Bliven (1999), Scatterometric signatures of multivariate drop impacts on fresh and salt water surfaces, *Int. J. Remote Sens.*, 20, 2149–2166.
- Stiles, B. W., and S. H. Yueh (2002), Impact of rain on spaceborne Ku-band wind scatterometer data, *IEEE Trans. Geosci. Remote Sens.*, 40(9), 1973–1983.
- Tharek, A. R., and J. Din (1990), Rainfall drop size distribution measurements in Malaysia, Fac. of Electr. Eng., Univ. Teknol., Skudai, Malaysia.
- Timothy, K., J. T. Ong, and E. B. L. Choo (2002), Raindrop size distribution using method of moments for terrestrial and satellite communication applications in Singapore, *IEEE Trans. Antennas Propag.*, 50(10), 1420–1424.
- Tsimplis, M., and S. A. Thorpe (1989), Wave damping by rain, *Nature*(342), 893–895.
- Tsimplis, M. N. (1992), The effect of rain in calming the sea, *J. Phys. Oceanogr.*, 22, 404.
- Uijlenhoet, R. (2001), Raindrop size distributions and radar reflectivity—Rain rate relationships for radar hydrology,

- Raindrop Size Distrib. Hydrol. Earth Syst. Sci.*, 5(4), 615–627.
- Weissman, D. E., and M. A. Bourassa (2008), Measurements of the effect of rain-induced sea surface roughness on the QuikSCAT Scatterometer Radar Cross Section, *IEEE Trans. Geosci. Remote Sens.*, 46(10), 2882–2894.
- Wetzel, L. B. (1990), On the theory of electromagnetic scattering from a raindrop splash, *Radio Sci.*, 25, 1183–1197.
- Wickerts, S. (1982), Drop size distribution in rain, report, Food and Agric. Org., Rome.
- Worthington, A. M. (1963), *A Study of Splashes*, reprint of 1910 publication, MacMillan, New York.
- Zhang, G., J. Vivekanandan, and E. Brandes (2001), A method for estimating rain rate and drop size distribution from polarimetric radar measurements, *IEEE Trans. Geosci. Remote Sens.*, 39(4), 830–841.
-
- L. F. Bliven, Wallops Flight Facility, NASA Goddard Space Flight Center, Wallops Island, VA 23337, USA. (francis.l.bliven@nasa.gov)
- C. Craeye and P. Sobieski, Telecommunications and Remote Sensing Laboratory, Université catholique de Louvain, B-1348 Louvain-la-Neuve, Belgium. (christophe.craeye@uclouvain.be; piotr.sobieski@uclouvain.be)